JOURNAL OF SPACECRAFT AND ROCKETS
Vol. 42, No. 6, November–December 2005

Closed-Loop Trajectory Simulation for Thermal Protection System Design for Neptune Aerocapture

Roman Jits,* Michael Wright,† and Y.-K. Chen‡
NASA Ames Research Center, Moffett Field, California 94035

A configuration for aerocapture at Neptune is considered with an emphasis on reduction of the overall aeroshell thermal protection system mass. The biconic vehicle is assumed to be capable of bank angle as well as angle-of-attack modulation for guidance and optimal trajectory shaping. A methodology is presented for determining a nominal trajectory that robustly accommodates off-nominal flight conditions with relatively small dispersions in integrated heat load. Such a trajectory, termed nominal robust, is presented for bank-only guidance. A nominal-robust trajectory is also generated for guidance with both angle-of-attack and bank modulation. Simulation of a nominal-robust trajectory with angle-of-attack modulation in the presence of multiple stacked off-nominal conditions is described. The resulting reduction of maximum heat rate and heat load relative to the undershoot and overshoot trajectories is quantified. The thermal protection system response based on closed-loop trajectory simulations for worst-case off-nominal scenarios is calculated and compared with the traditional overshoot/undershoot thermal protection system design method. The results show that the use of the nominal-robust methodology results in a significant decrease in aeroshell mass, and that combined bank and angle-of-attack modulation further reduces trajectory dispersion and stagnation-point-integrated heat load as compared to pure bank-angle modulated trajectories.

Nomenclature

C_D	=	drag coefficient
C_L	=	lift coefficient
C_3	=	Earth departure energy, km^2/s^2
M_e	=	edge Mach number
Q_{con}	=	convective heat load, J/cm^2
Q_{rad}	=	radiative heat load, J/cm^2
q_{con}	=	convective heating rate, W/cm^2
q_{rad}	=	radiative heating rate, W/cm^2
Re_θ	=	momentum thickness Reynolds number
α	=	trim angle of attack, deg
β	=	ballistic coefficient, kg/m^2
γ_{entry}	=	entry angle, deg
ΔV	=	propulsive velocity change, m/s

Introduction

AEROCAPTURE is currently under investigation by the NASA In-Space Propulsion program as a potentially enabling technology for missions to Neptune.[1] Aerocapture is a technique that uses a single, aerodynamically controlled pass through the planetary atmosphere that dissipates sufficient energy to capture the spacecraft into the desired closed, elliptical orbit about the target body. Thus, an aerocapture vehicle replaces the large propulsion system necessary for a traditional orbit insertion with the potentially much smaller mass of an aeroshell and thermal protection system (TPS) to protect the spacecraft from the entry heating environment. Once the vehicle leaves the atmosphere, a small propulsive maneuver is performed to raise the orbit periapse to the desired altitude and prevent reentry into the atmosphere. The potential benefit of aerocapture can thus be maximized by minimizing the entry heat load (and therefore the aeroshell mass) and the postexit periapse raise ΔV (propellant mass). Aerocapture has been studied extensively over the past decades and has repeatedly been shown to produce significant payload gains for missions to atmosphere-bearing bodies.[2] For a lifting entry, the range of possible entry angles that permits a successful orbit insertion, defined as the entry corridor, is bounded by the undershoot limit, which is the steepest entry angle achievable for the desired postexit apoapse, and by the overshoot limit, which is the shallowest entry angle resulting in the same postexit apoapse. The undershoot limit is determined by assuming that the vehicle flies the entire trajectory with an upward pointed lift vector; the overshoot limit is determined by a full lift-down orientation. For a fixed postexit apoapse, the width of the entry corridor is mainly a function of the lift-to-drag ratio (L/D) of the entry vehicle, its entry velocity and, to a lesser degree, its ballistic coefficient.

In practice, the entry corridor that is used for design is reduced from its ideal width to accommodate entry navigation (delivery) errors as well as dispersions in the atmosphere of the target planet. A lifting aerocapture vehicle can use its lateral force to compensate for these uncertainties by rolling the lift vector about the velocity vector, a control technique known as bank or roll modulation. In this way the spacecraft can fly anywhere between a full lift-up and full lift-down orientation as required. An additional control option is to vary the angle of attack (AOA) during the entry (AOA modulation), which improves control authority by changing the vehicle L/D and ballistic coefficient. The guidance algorithm directs the control system to change the vehicle orientation as required during the aeropass in order to achieve the desired postexit orbital apoapse and inclination. To account for realistic off-nominal conditions, the entry vehicle must implement a closed-loop guidance algorithm. Simulation of a vehicle flying with closed-loop guidance requires two loops of the trajectory model: an outer and inner loop. The outer loop simulates the vehicle flight in off-nominal conditions. The inner loop represents the onboard guidance system that predicts the remainder of the trajectory based on current information. Control commands are derived and issued from the inner loop, which then affect the vehicle flight being simulated in the outer loop. An open-loop trajectory simulation is not adequate for this purpose because off-nominal conditions are not known a priori, and there is no guidance feedback mechanism.

Received 14 September 2004; revision received 15 December 2004; accepted for publication 19 January 2005.

*Postdoctoral Associate, National Research Council; currently Research Scientist, MS 230-2, Reacting Flow Environments Branch, Eloret Corporation. Member AIAA.

†Senior Research Scientist, MS 230-2, Reacting Flow Environments Branch. Senior Member AIAA.

‡Senior Research Scientist, MS 234-1, Thermal Protection Materials Branch. Senior Member AIAA.

The TPS requirements for any aerocapture mission are defined by the maximum heating rate, which dictates the choice of the material for the exposed surface of the vehicle, and the integrated heat load accumulated throughout the aeropass, which dictates the thickness of the TPS material. Traditionally, the maximum heat rate from the undershoot trajectory and the maximum heat load from the overshoot trajectory are used for design.[3] However, these values can be extremely conservative for many applications, leading to a needlessly heavy aeroshell design. A more sophisticated design approach is to use Monte Carlo techniques to model the entry trajectory in the presence of realistic dispersions.[4] The design heat flux and heat load are then determined statistically by running (potentially) thousands of trajectories, which can be a time-consuming process.

For missions to Neptune, large uncertainties in atmospheric models combined with entry navigation errors (because of Neptune's remote location) significantly reduce the size of the entry corridor. Therefore, an efficient guidance algorithm capable of producing optimal (minimum TPS mass) trajectories in response to a variety of off-nominal conditions is very important for optimal aerocapture at Neptune. An appropriate choice for this purpose would be a predictor-corrector type of algorithm in which information about the current state of the vehicle is used to predict the resulting exit state, and control commands are issued as needed to minimize predicted exit errors. Furthermore, to shorten transit time and to ensure a practical entry corridor width, aerocapture at Neptune necessitates high-entry velocities, which translates into high integrated heat loads, challenging TPS design requirements, and a large TPS mass fraction (ratio of TPS mass to total entry mass). These challenges make aerocapture at Neptune a difficult problem and highlight the need for improvements in trajectory design. An ideal nominal aerocapture trajectory would have low dispersions in peak heat rate and integrated heat load in the presence of extreme atmospheric dispersions and approach guidance errors, without a significant increase in propulsive requirements for postaerocapture orbit adjustments. The nominal-robust trajectory[5] approach offers a solution for an entry vehicle that uses its available lifting control authority to design such a nominal trajectory. Further details on the nominal-robust trajectory approach can be found in Refs. 5 and 6. Thus designed nominal-robust trajectory is simulated including multiple combinations of stacked worst case off-nominal conditions via a closed-loop numerical predictor corrector guidance algorithm. It must be emphasized that this approach to simulating off-nominal trajectories is not as mathematically rigorous as a Monte Carlo dispersion analysis.[4] However, although not encompassing all possible combinations of off-nominal conditions, the approach adopted here offers the advantage of quickly identifying the TPS design envelope in terms of realistic maximum stagnation-point heat rates and heat loads. Also, because this approach uses stacked dispersions as the worst case, it is likely that the resulting analysis will be conservative, meaning that the simulated trajectories will be beyond the $n-\sigma$ envelope of expected dispersions from a true Monte Carlo analysis. These features make the nominal-robust trajectory method attractive for preliminary design activities, whereas full Monte Carlo analysis remains the standard for detailed design.[4]

The nominal-robust trajectories computed in this work will be used to size a TPS for this mission, and the TPS mass will be compared to that determined via a traditional approach using the overshoot and undershoot trajectories. Also included is an evaluation of the use of AOA modulation to further reduce trajectory dispersions and thus reduce heat loads beyond the level achievable with bank-only guidance. It is clear that the capability to modulate AOA will facilitate guidance of the vehicle, but the degree to which it is beneficial in terms of TPS mass reduction is quantified in this work.

Mission Scenario

One of the main difficulties regarding Neptune is its remote location in the solar system. Trans-Neptune trajectories with minimum Earth departure energy C_3 have a flight time of more than 30 years. To shorten the duration, while using a launch vehicle with the same C_3 capability, a high-specific-impulse propulsion system needs to be used during transit to Neptune. However, shorter transit times result in high entry velocities at Neptune, ranging from 29 to 32 km/s for trip times of 12–10 years, respectively.[3] In the present study, the entry velocity of 29 km/s is considered to identify trends in trajectory design and the resulting TPS material response. The target orbit for aerocapture insertion is chosen to be coplanar with that of Neptune's largest moon Triton, with an apoapse of 400,000 km, enabling close encounters with the moon for scientific observation. Thus, the mission profile consists of a single aerodynamically controlled atmospheric pass to capture the vehicle into elliptic orbit with exit apoapse altitude of 400,000 km and the same inclination as at entry (inclination = 157.3 deg). Then, as the vehicle reaches apoapse, it performs a propulsive burn to raise its postatmospheric exit periapse to 1000 km above the zero-altitude reference point (1 bar atmospheric pressure).

Preliminary Vehicle Concept

For aerocapture at Neptune to be successful, the configuration of the entry vehicle should be chosen to provide an entry corridor width adequate to accommodate all of the off-nominal factors that are bound to be present throughout the aeropass. The requirement to aerocapture into a long elliptical orbit means the entry corridor width will strongly depend on the entry velocity. On one hand, the entry angle of the overshoot trajectory, which will produce a high apoapse, is much less sensitive to a variation of entry velocity than the entry angle of the undershoot trajectory targeted to produce the same apoapse altitude. On the other hand, a high apoapse significantly limits the depth of the undershoot trajectory and thus the corridor width, which in turn can limit the vehicle's ability to compensate for dispersions. Therefore, the lower bound on entry velocity (29 km/s) is of particular interest because for a given vehicle configuration the corridor width will increase with entry velocity.

Vehicle configuration trades previously carried out for a 29-km/s entry showed that in order to provide an adequate corridor width, a vehicle with a L/D of at least 0.8 is required.[3] Given the remote location of Neptune, it is likely that entry navigation errors will be larger than those for inner-system planets; thus, for this study the entry angle error was assumed to be ± 0.5 deg (Ref. 7). It might seem logical that a vehicle with higher L/D could provide the necessary maneuverability to compensate for this navigation error. However, increasing L/D typically increases the ballistic coefficient as well (by reducing drag), and as a result such a vehicle would experience higher integrated heat load. It will also be less volumetrically efficient. The net result will be an increase in TPS mass fraction. Therefore, an L/D of about 0.9 was deemed to be a reasonable compromise between the control authority it can provide and the need for efficient TPS design. The chosen configuration is one of the candidate entry shapes considered by Wercinski et al.[3] for application to Neptune aerocapture. It is a biconic vehicle with L/D of 0.88 at $\alpha = 36$ deg, shown in Fig. 1. With the assumption of a Delta class launch vehicle delivering a total Neptune entry mass of 600 kg, this biconic vehicle has a ballistic coefficient of $\beta = 609$ kg/m^2 at the trim angle of attack.

Angle-of-Attack Modulation

Traditionally, aerocapture vehicles are assumed to be controlled through bank modulation alone. However, if the entry vehicle were capable of modulating the angle of attack as well it might be possible to further optimize the entry trajectory and reduce total heat load. The theoretical advantages of angle-of-attack modulation for Neptune aerocapture will be quantified in this study. It is clear

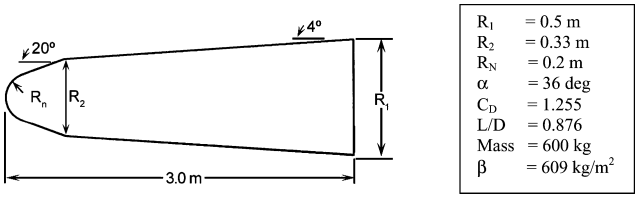

Fig. 1 Biconic vehicle geometry.

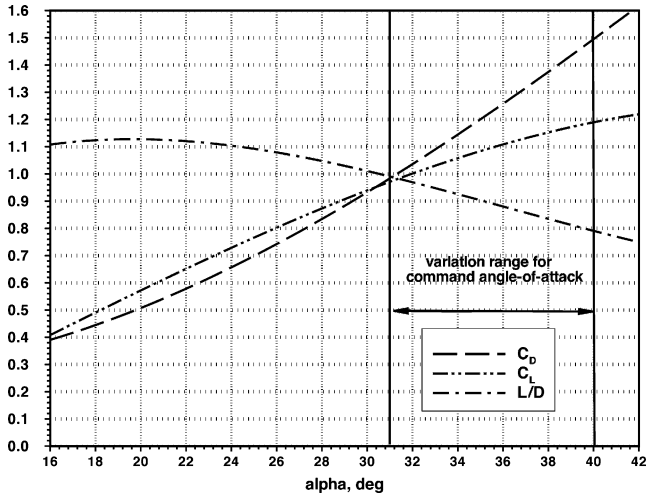

Fig. 2 Real-gas aerodynamic data for biconic vehicle (from Ref. 3).

that there are significant engineering hurdles that will make it difficult to implement AOA modulation on any aerocapture vehicle. This paper will not discuss the specifics of the implementation of such a system, but will help to determine if the engineering complexity of such a control system could be justified by reductions in TPS mass and in dispersions in vehicle state at atmospheric exit.

The addition of AOA modulation capability has two consequences. First, it provides guidance benefits. In the initial phase of aerocapture, a vehicle capable of AOA modulation can fly at lower AOA to widen the corridor width. Later, especially during the exit leg of the trajectory when the pullout maneuver is initiated, AOA and hence drag coefficient C_D can be modulated effectively to control the altitude of the exit apoapse. At the same time, bank modulation can be used throughout the exit phase primarily to achieve the desired exit orbital inclination. Besides guidance enhancement, AOA modulation can also be used to reduce the heat load accumulated by the vehicle. To achieve these benefits, the AOA variation range must be large enough to enable the aerocapture vehicle to reduce its ballistic coefficient significantly while flying at lower altitudes, where most of the heating occurs. For this study, the AOA variation range is chosen to be between 31 and 41 deg, or ± 5 deg from the nominal trim angle of 36 deg. This allows a C_D change of more than 50%, from 1.0 at 31 deg to 1.55 at 41 deg, as shown in Fig. 2. Real gas aerodynamic properties of this shape were computed in Ref. 3.

Closed-Loop Trajectory Simulation

The closed-loop trajectories generated in this work are obtained via a predictor-corrector-type guidance algorithm. In this algorithm, an initial set of controls in the beginning of the aeropass is first computed for the nominal trajectory assuming that no dispersions are present. As the vehicle flies along this trajectory, the guidance algorithm periodically checks (predicts) if prescribed tolerances on the desired apoapse altitude and orbital inclination at atmospheric exit are violated as a result of encountered dispersions. When these tolerances are violated, the algorithm modifies (corrects) the bank angle and/or AOA to offset the effects of the dispersions and then computes the remainder of the new trajectory based on the current information. This process is repeated at regular time intervals throughout the aeropass maneuver until the vehicle exists the atmosphere. Another way to think about this algorithm is as an inner and outer loop of the trajectory simulation. The outer loop tracks the current trajectory including the integrated effects of all off-nominal conditions previously encountered. Whenever a change is required, the inner loop, containing the predictor-corrector guidance algorithm, engages and determines the adjustments that should be made to the controls and how those changes will affect the remainder of the trajectory. The trajectory simulations in this work are performed using the three-degree-of-freedom Program to Optimize Simulated Trajectories (POST).[8] This code is used for both the inner and outer loop of the simulation.

The outer-loop POST is used to simulate the trajectory of the vehicle in the perturbed environment, where all off-nominal conditions are modeled. POST uses fourth-order Runge–Kutta numerical integration to obtain the position and velocity of the vehicle throughout the aeropass. In the outer loop, the aerocapture trajectory is simulated in 5-s time intervals, and at the end of each interval the current state vector of the vehicle is passed to the inner loop of the simulation.

The inner-loop POST is used to numerically integrate the trajectory from the vehicle state received from the outer loop to the atmospheric exit. Thus, the inner-loop generated trajectory is called the predicted trajectory and is used to evaluate whether the exit conditions (defined by orbital apoapse and inclination at atmospheric exit) are within prescribed tolerances, as well as to check if the stagnation-point integrated heat load exceeds the design limit. If these constraints are violated, then the inner-loop POST steepest descent algorithm is used to target (correct) the predicted trajectory to the desired orbital apoapse and inclination and keep stagnation-point heat load below its limit. The steepest descent algorithm performs this targeting by perturbing the controls, and the new trajectory is generated by the inner loop in an iterative manner until the exit conditions and prescribed limit on heat load are met (Fig. 3). After targeting is completed, the values of all independent control parameters associated with the targeted solution are used as the initial guess by the inner loop to propagate the trajectory from the new vehicle state to the atmospheric exit in the next guidance cycle. The two initial controls from the targeted solution are passed as command controls back to the outer loop, where they are implemented as bank-angle and angle-of-attack commands for the aerocapture vehicle.

Thus, in the outer loop the trajectory of the vehicle is simulated with these command controls during the current guidance interval until new command bank and angle of attack are passed from the next inner-loop guidance cycle. During the next guidance interval, the trajectory is thus simulated with the new command bank and angle of attack. In the outer loop the bank angle and angle of attack are assumed to change instantaneously, as the modeling of the controller and optimization of the associated control law are beyond the scope of this work. The length of the guidance update interval is set at 5 s to address computational delays caused by trajectory targeting and to allow time for execution of the commanded bank and alpha. It is assumed, based on the trajectory simulations, that out of five seconds one second is allocated for the trajectory computation and the remaining four seconds are used to execute the commanded attitude change.

It is understood that by modeling changes in vehicle attitude as occurring instantaneously we are not accounting for inertial effects

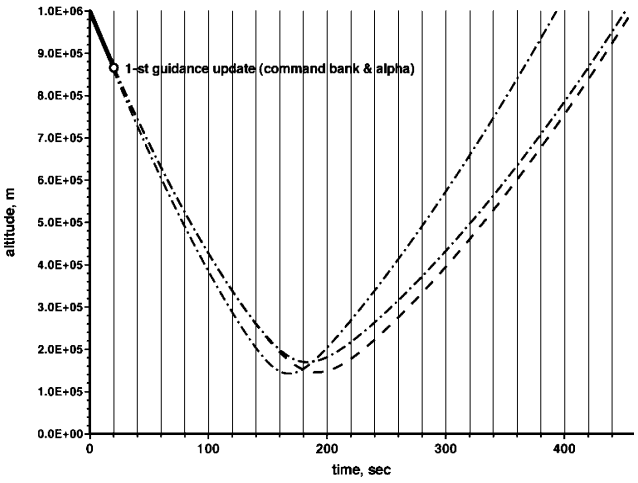

Fig. 3 At the end of current guidance interval, trajectory is iterated to meet desired exit conditions.

and resulting delay in response to guidance commands. For example, a roll-reversal maneuver (when a change in bank angle close to 180 deg is required) can take almost 10 s, assuming a maximum roll rate of 20 deg/s, a typical value for conceptual aerocapture vehicles. The result of this delay is degraded performance of the guidance algorithm over the theoretical limit, which manifests primarily as increased postexit ΔV. This effect will be most pronounced when multiple roll reversals are used as a means for control of orbital inclination on the exit leg of the trajectory. However, the proposed guidance scheme as detailed in the following section actually minimizes the adverse effects of such control system delays because there is always only one bank reversal, executed near minimum altitude. Only a single roll reversal is required because of the ability of the proposed guidance scheme to use multiple simultaneous controls to target the vehicle to the desired exit apoapse and inclination during every guidance cycle, throughout the entire trajectory. As a result, there is no need to use multiple roll reversals to correct errors in orbital inclination, as would be the case in the classical dead-band approach, when inclination is corrected on the exit part of the trajectory after apoapse targeting is mostly completed.

Guidance Algorithm Macrologic

The guidance algorithm is written as an additional subroutine to the inner loop of the trajectory simulation. The guidance algorithm controls data exchange between the outer and inner loops of the simulation, modifies controls generated by the inner-loop POST targeting routine, and feeds them back into the main simulation loop.

The key feature of this algorithm is its guidance scheme, in which the aeropass is divided into four time phases. At the beginning of the each time phase, the bank angle and angle of attack are implemented, as shown in Fig. 4. The first phase is entry, where the vehicle is guided primarily to compensate for dispersions in entry angle. Second is the maximum deceleration phase, where most of the energy dissipation occurs and the guidance compensates primarily for off-nominal atmospheric density and vehicle aerodynamic dispersions. Third is the pull-out maneuver phase when a bank reversal is executed to null out most of change in orbital inclination resulting from the lateral component of bank modulation in the two previous phases. Fourth is the exit phase during which bank angle and angle of attack are used to drive orbital apoapse and inclination to the target values within prescribed tolerances at atmospheric exit. Thus, to generate an initial trajectory, 11 independent control parameters are used by the inner loop: the first pair of bank angle and angle of attack at the current time from which the trajectory is propagated by the inner loop, three other pairs of bank angle and angle of attack at each of the three future phases, and three (variable) times at which each of these phases will begin. As the outer-loop simulated trajectory (vehicle flying in the perturbed environment) progresses toward atmospheric exit, the bank angle and alpha for the current time in the inner loop assume the corresponding values of the next pair of bank angle and alpha in the guidance scheme. So, the total number of controls stays at 11 at any time, but the number of "active controls" (those from the current phase plus from future phases) changes from 11 in the first phase to nine in the second, six in the third, and finally to three in the last phase. Thus, the number of active controls used by inner-loop targeting routine (steepest descent gradient algorithm) in the current phase is always more than two. This strategy provides a significant advantage in meeting prescribed constraints as compared to a traditional guidance scheme, which would have only one or two controls (bank angle, or bank angle and alpha if AOA modulation is employed).[9] This approach offers the flexibility of steepest descent gradient targeting, which is not constrained to drive the vehicle to a reference trajectory, but instead compensates for encountered dispersions by producing a new trajectory with the desired exit state. This capability of the proposed guidance scheme is its main distinction from traditional reference trajectory-based guidance algorithms such as hybrid predictor-corrector aerocapture scheme,[10] in which despite an analytically predicted exit state only one or two controls (depending on whether alpha modulation is employed) are used to drive the vehicle back to the reference trajectory parameters.[10] In the guidance scheme proposed herein, the steepest descent gradient targeting algorithm employs multiple controls to enable targeting the desired exit apoapse and inclination throughout the trajectory and has enough flexibility to also continuously track an additional trajectory constraint (such as maximum integrated heat load). Given that aerocapture missions to Neptune will be characterized by a very large total heat load,[11] this capability represents an important advantage. The algorithm is shown in flowchart form in Fig. 5.

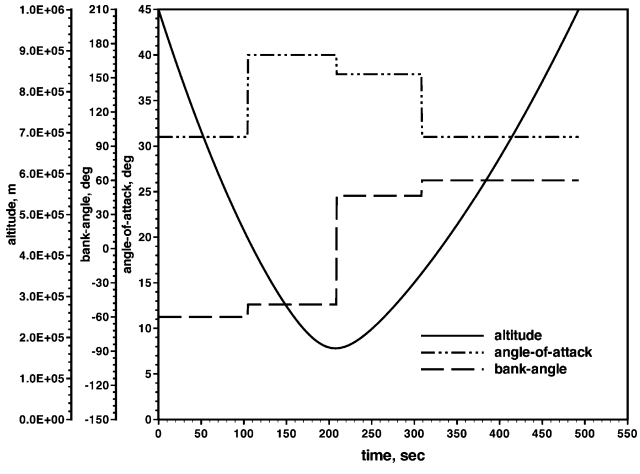

Fig. 4 Time histories for nominal-robust trajectory with bank and angle-of-attack modulation.

The guidance algorithm also has a structure of prioritized heuristic rules, which is engaged by the inner-loop targeting routine, depending on a combination of the vehicle state, stagnation-point heat load, ambient density, and atmospheric exit conditions. Structurally the algorithm consists of four parts, with each part engaging as needed depending on the predicted conditions at atmospheric exit. Thus, during each guidance cycle the inner loop receives the new vehicle state from the outer loop and uses the set of 11 controls found in the previous guidance cycle as a first guess to propagate the trajectory to the atmospheric exit in the first iteration. During subsequent iterations, these controls are perturbed to target this trajectory to the desired apoapse altitude and orbital inclination within prescribed tolerances. If the resulting trajectory violates the maximum heat load constraint, the first part of the guidance algorithm is engaged, and it modifies the controls in order to meet this constraint during the remaining iterations in the guidance cycle. However, there are situations when the trajectory cannot be successfully propagated to atmospheric exit or the vehicle cannot be captured into a closed elliptic orbit due to a combination of the current state, atmospheric density, and the control settings from the previous guidance cycle. The former case produces a trajectory in which the vehicle hits the planetary surface (specified as an atmospheric pressure of 1 bar), and causes the targeting routine to stop. The latter case results in a trajectory in which the vehicle exits the atmosphere with hyperbolic orbital energy, thus causing the targeting routine to stop because the specified limit on maximum trajectory time is violated. These stopping conditions are used as engagement flags for the second or third part of the guidance algorithm, which modify the current controls in such a way that either the trajectory is propagated to atmospheric exit or the vehicle is captured into a closed elliptic orbit. For example, in the case of hyperbolic skip-out the guidance algorithm increases the angle of attack and directs the lift vector more downwards every iteration until a converged solution is obtained. Thus overridden by the guidance algorithm, the modified controls find a targeted solution in a new guidance cycle within five iterations for most combinations of vehicle state, atmospheric density, and exit conditions. Further details on the scheme of the guidance algorithm can be found in Ref. 12.

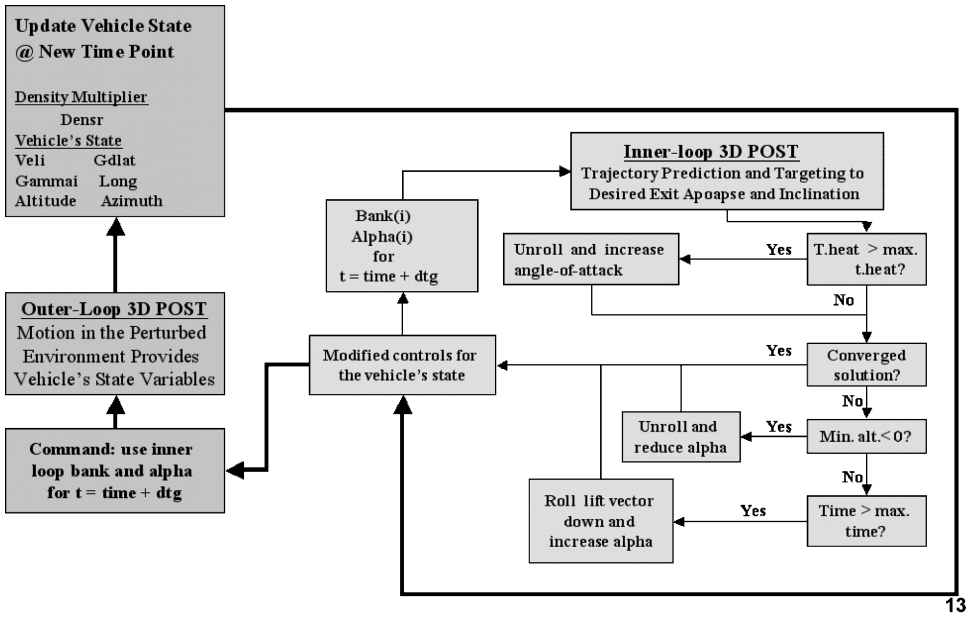

Fig. 5 Guidance algorithm flowchart.

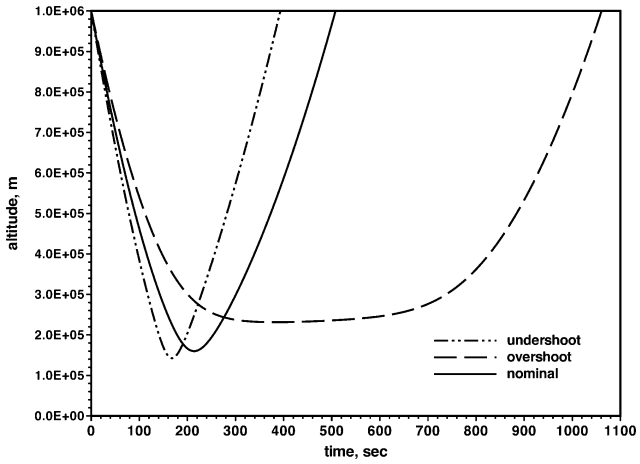

Fig. 6 Overshoot, undershoot, and nominal trajectory altitude time histories.

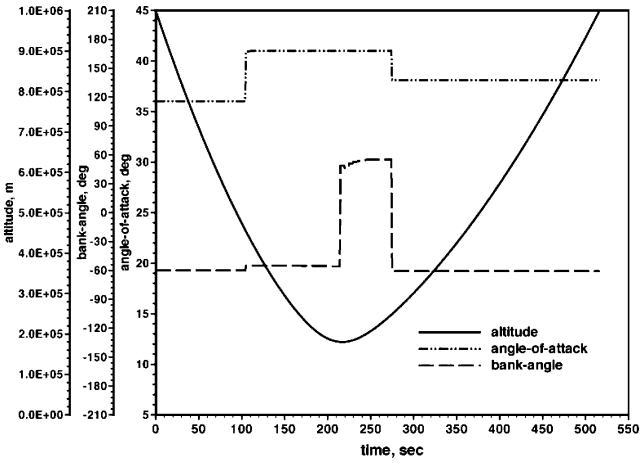

Fig. 7 Bank-angle and angle-of-attack control time histories for nominal case.

Nominal Trajectory

All trajectory simulations were carried out for a retrograde equatorial entry into a rotating Neptune atmosphere (81% H_2 and 19% He by volume). A retrograde entry was chosen to facilitate observation of Neptune's largest moon, Triton. Atmospheric properties as a function of altitude are based on the Yelle model.[13] The aerocapture corridor is bounded by the overshoot and undershoot trajectories. In this study, the overshoot trajectory for a given angle of attack is defined as that which has the shallowest entry angle that permits a postatmospheric exit apoapse altitude of 400,000 km and the same orbital inclination as the one at entry. For lifting vehicles, the shallowest entry angle is achieved by flying constantly with full lift vector down. Similarly, the undershoot trajectory is defined as full lift-up, which has the steepest entry angle that still produces the required postatmospheric exit state. Figure 6 shows the overshoot and undershoot trajectories for the baseline biconic vehicle with an angle of attack of 36 deg. For a 29-km/s entry, the resulting corridor width is 2.47 deg at 1000-km altitude, which is adequate for accommodating possible entry navigation errors and atmospheric dispersions (assumed to be ± 0.5 deg of nominal entry angle and $\pm 30\%$ of nominal atmospheric density accordingly). Time-varying dispersions in atmospheric conditions are beyond the scope of this work, but can certainly be accommodated via a Monte Carlo approach.

The nominal trajectory for this case is defined by assuming that the vehicle enters in the middle of the aerocapture corridor with no atmospheric dispersions encountered during the aeropass. Entering in the middle of the corridor maximizes the ability of the vehicle to compensate for dispersions. The initial AOA was set at an intermediate value ($\alpha = 36$ deg) to maximize control authority. The entry bank angle was chosen to be 60 deg (slightly lift-up) rather than 90 deg to reduce both heat load and the amount of bank modulation required to achieve the desired apoapse. Figure 7 shows the resulting trajectory, assuming both bank and AOA modulation. The guidance algorithm commanded the angle of attack to increase to its maximum value of 41 deg through the middle phase of the trajectory, where most of the aerodynamic deceleration occurs, reducing the ballistic coefficient and allowing the vehicle to fly at higher altitudes and thus accumulate a smaller heat load. Throughout the exit leg of the trajectory, the AOA was lowered to 38 deg to reduce drag and achieve the desired orbital apoapse, with resulting postexit ΔV of only 28 m/s required to raise the periapse to 1000 km.

From Table 1 we see that the resulting stagnation-point heat load of the nominal trajectory is 50% lower than that of the overshoot. Figure 7 shows that the bank angle remains between ± 60 deg throughout the entry, which corresponds to an upward-directed lift vector (in this study a bank angle of 0 deg is defined as full lift-up and 180 deg as full lift-down). Maintaining this orientation is an important advantage, because it permits enough control authority for bank modulation to compensate even for severe off-nominal conditions

Table 1 Parameters of simulated trajectories

Trajectory	γ_{entry}, deg	$\rho\times$ factor	$C_{D\,\text{nom}}$ $\times$ factor	$C_{L\,\text{nom}}$ $\times$ factor	Normalized heat rate	Normalized heat load	Min. alt., km	Time, s	Exit apoapse (km $\times 10^5$)	ΔV, m/s
Overshoot	−11.360	0.7	1.0	1.0	0.40	1.00	223	1014	3.99	20
Undershoot	−13.827	1.3	1.0	1.0	1.00	0.47	167	412	4.01	35
Nominal	−12.594	1.0	1.0	1.0	0.73	0.50	180	516	4.01	28
1A	−12.094	0.7	0.9	0.95	0.75	0.56	165	591	4.30	69
2A	−13.094	1.3	1.1	1.05	0.81	0.49	180	473	3.76	73
3A	−12.094	1.3	1.1	1.05	0.71	0.50	191	508	3.98	30
4A	−13.094	0.7	0.9	0.95	0.89	0.51	153	496	4.14	49
5A	−12.094	0.7	1.1	1.05	0.71	0.49	166	539	3.92	40
6A	−13.094	1.3	0.9	0.95	0.96	0.55	171	470	4.07	39
7A	−12.094	1.3	0.9	0.95	0.74	0.56	189	567	4.20	54
8A	−13.094	0.7	1.1	1.05	0.83	0.48	156	476	3.92	43
1B	−12.094	0.7	0.9	0.95	0.77	0.66	162	658	4.33	71
2B	−13.094	1.3	1.1	1.05	0.89	0.48	175	443	3.58	114
3B	−12.094	1.3	1.1	1.05	0.90	0.50	174	481	3.85	57
4B	−13.094	0.7	0.9	0.95	0.94	0.54	148	519	4.23	60
5B	−12.094	0.7	1.1	1.05	0.73	0.56	167	557	3.75	73
6B	−13.094	1.3	0.9	0.95	0.95	0.55	171	511	4.26	72
7B	−12.094	1.3	0.9	0.95	0.95	0.60	176	575	4.25	61
8B	−13.094	0.7	1.1	1.05	0.88	0.48	152	463	3.48	136

and still direct the vehicle to desired conditions at atmospheric exit. The stagnation-point heat rate and heat load are estimated using the POST stagnation-point heating correlations, which were derived for air. It is assumed that the air correlation will be sufficient to examine trends, although the absolute magnitude of the heating values will be incorrect for Neptune entries. Therefore, values for heat rate and load in Table 1 are normalized by the reference overshoot and undershoot trajectories, respectively. The validity of this assumption will be demonstrated in the next section, where the full three-dimensional aerothermal environment is simulated for a representative set of the trajectories in Table 1 using computational fluid dynamics with an appropriate nonequilibrium thermochemical model for Neptune.

Nominal-Robust Trajectories with Constrained Heat Load

The next step is to simulate the entry trajectory in the presence of dispersions. As stated earlier, the intention is to produce a nominal-robust trajectory that is able to handle extreme off-nominal conditions while still having a minimum heat load and postexit ΔV. Therefore, it is desired to constrain the heat load to some reasonable level during the trajectory analysis. To select an appropriate constraint, we note that it is possible to reduce the heat load below that accumulated on the nominal trajectory. However, with AOA already kept at its maximum at lower altitudes, this reduction can be accomplished only with a bank-angle sequence even closer to a full lift-up orientation, which will be done at the expense of trajectory robustness, meaning here the ability to compensate for imposed off-nominal conditions.[6] Thus, for all off-nominal trajectory simulations, the constraint on maximum stagnation-point heat load was set to that of the nominal case (approximately 50% of the overshoot value). In practice, the minimum achievable heat load for a given trajectory was often somewhat larger than the targeted maximum because of the effects of the large imposed dispersions.

Simulations were carried out for the eight critical dispersion combinations described in Table 1 (cases 1A–8A). All dispersions were modeled in the outer loop. Modeled dispersions included errors in entry angle of ± 0.5 deg, shifts in atmospheric density profile of $\pm 30\%$ from nominal density, and ± 2-deg misprediction of the aerodynamic trim angle. Aerodynamic dispersions were modeled using multipliers on the baseline ($\alpha = 36$ deg) lift-and-drag coefficients. Thus, a higher than nominal trim angle was modeled using C_L of 1.05 and C_D of 1.1, and a lower than nominal trim angle was modeled using C_L of 0.95 and C_D of 0.9.

As can be seen from Table 1, all simulated off-nominal combinations were composed from maximum values for expected uncertainties. Cases 1A and 2A represent worst-case stacked uncertainties; in case 1A the vehicle enters at a shallow entry angle and flies through a thin atmosphere with reduced drag coefficient, whereas in case 2A a steep entry angle is combined with a dense atmosphere and higher drag. There is a little probability that these extreme combinations will be encountered in reality, but this was done intentionally in order to stress the vehicle guidance algorithm. The other off-nominal trajectories are also taken from maximum values of expected uncertainties, but they are composed in a random manner. Modeling these extreme off-nominal cases allows us to evaluate the sensitivity of the guidance algorithm to combined maximum dispersions and to determine its robustness.

To evaluate the relative effectiveness of AOA modulation, identical combinations of off-nominal conditions were modeled for bank-only modulated trajectories using the same closed-loop guidance algorithm (in this case with eight independent parameters rather than 11). These cases are also listed for comparison in Table 1 (cases 1B–8B). The guidance algorithm for both the bank and AOA and bank-only modulated cases was constrained to stay below the stagnation-point heat load of the nominal trajectory, or 50% of the heat load of the reference overshoot trajectory, if possible.

As seen from Table 1, aerocapture for all off-nominal cases was successful. The bank and AOA modulated cases have significantly smaller dispersions in postexit ΔV than those using bank modulation only (43 vs 79 m/s). In addition, the maximum postexit ΔV required for the bank and AOA modulated cases is significantly lower (73 vs 136 m/s). In that case, a steeper than nominal entry angle was combined with higher than nominal trim angle and atmospheric density. To compensate for these off-nominal conditions, the guidance algorithm profiled the angle of attack so that it was near maximum through the phase of maximum deceleration (see Fig. 8). At the onset of the pullout maneuver, the AOA was lowered in the successive guidance cycles to its minimum value to reduce errors in postexit apoapse. The bank-only modulated trajectory (case 2B) for the same off-nominal conditions produced a larger error in postexit apoapse, which required a 114-m/s velocity increment for the correction. It must be emphasized, however, that even the largest postexit ΔV of 136 m/s (case 8B) can be acceptable in practice because it is small compared to the overall velocity reduction of about 6400 m/s achieved via the aerocapture maneuver. Nevertheless, comparison of dispersions in postexit ΔV shows that addition of AOA modulation capability to the guidance scheme indeed results in improved performance. The extent to which this improved performance impacts the overall vehicle can only be determined through a complete systems analysis.

Examination of the stagnation-point heat loads in Table 1 reveals that the maximum heat load target (50% of the reference overshoot value) was met about half the time in the trajectories that included

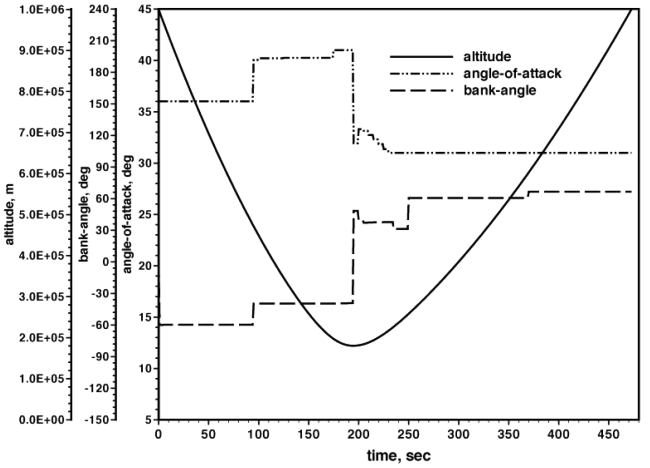

Fig. 8 Time histories for case 2A with nominal −0.5-deg entry angle, 130% of nominal density, and +2.0-deg error in trim angle.

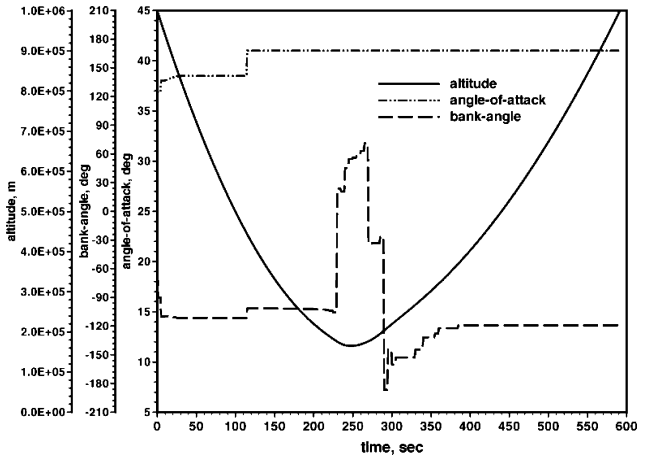

a) Case 1A, bank and AOA modulation

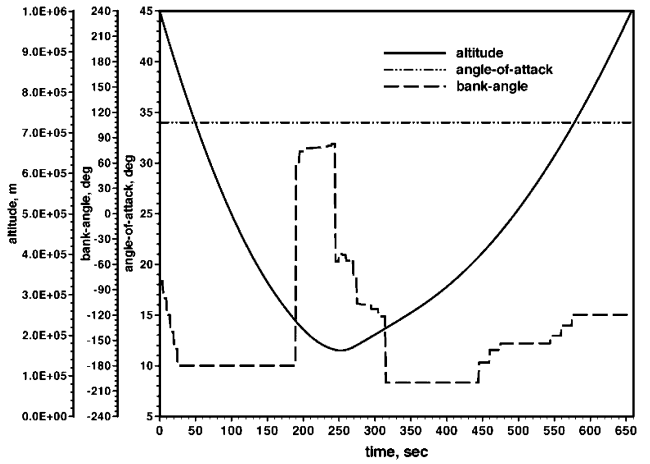

b) Case 1B, bank-only modulation

Fig. 9 Time histories for nominal +0.5-deg entry angle, 70% of nominal density, and −2.0-deg error in trim angle.

dispersions. Of the bank and AOA modulated cases the trajectories with the highest stagnation-point heat load are cases 1A and 7A. For these cases the heat load is 44% less than for the reference overshoot trajectory. For the bank-only modulated cases, the trajectory with the highest heat load (34% less than overshoot) is case 1B. Figure 9a shows the computed trajectory for case 1A. Because of lower than nominal density and drag and shallow entry angle, the guidance algorithm kept the commanded AOA at its maximum value of 41 deg through most of the trajectory to dissipate the necessary energy required to reach the target apoapse. The lift vector was downward directed through most of the trajectory as well, except for a brief period at minimum altitude where the pullout maneuver was initiated. Because in the bank-only modulation cases the vehicle flies at a predetermined trim angle and drag cannot be increased, the guidance algorithm could only reorient the direction of lift vector to compensate for the same dispersions. Indeed, as seen from Fig. 9b, the bank angle for case 1B was kept essentially at a lift-down position (−180 deg) through most of the trajectory, again, with exception of the lower-altitude phase where the roll-reversal and pull-out maneuvers were executed.

High-Fidelity TPS Sizing

A high-fidelity analysis is required to evaluate the distributed TPS thickness required for each case. Therefore, full three-dimensional CFD solutions are computed on the overshoot trajectory as well as off-nominal cases 1A and 1B (see Table 1). For each trajectory, solutions are generated at eight to 10 instants to simulate the heating pulse. A TPS sizing is then computed at four selected body points on the vehicle to determine the TPS thicknesses for each candidate trajectory. The points selected are the stagnation point (#1), the midpoint of the first (#2), and second (#3) cones on the wind centerline, and the midpoint of the first cone on the leeward centerline (#4). The locations of these points are shown in Fig. 10. Because of the high heat fluxes expected on the windward side, the baseline TPS material is fully dense carbon-phenolic, analogous to that used on the Pioneer Venus and Galileo missions. Carbon-phenolic was determined to be the only viable existing material for the anticipated windward side Neptune aerocapture heating environment in a previous study.[14]

The CFD solutions are computed using the data-parallel line relaxation code (DPLR).[15] DPLR is a parallel multiblock reacting flow Navier–Stokes solver developed at the NASA Ames Research Center, which has been used previously for many planetary entry applications, including Neptune aerocapture.[3,11] The gas is modeled with a five-species (H_2, H, H^+, He, e), finite rate chemistry model. Other trace atmospheric species (primarily CH_4 and N_2) are neglected for this work, as they were previously shown to have a negligible impact on aeroheating.[11] Reaction rates are taken from Leibowitz and Kuo[16] and were based on shock-tube data for H_2/He shock waves in this velocity range. The flowfield around the vehicle is assumed to be laminar throughout the heat pulse, an assumption that will be discussed further. The surface is assumed to be fully catalytic to H atom and ion recombination. A radiative equilibrium wall boundary condition is enforced, with an emissivity of 0.85.

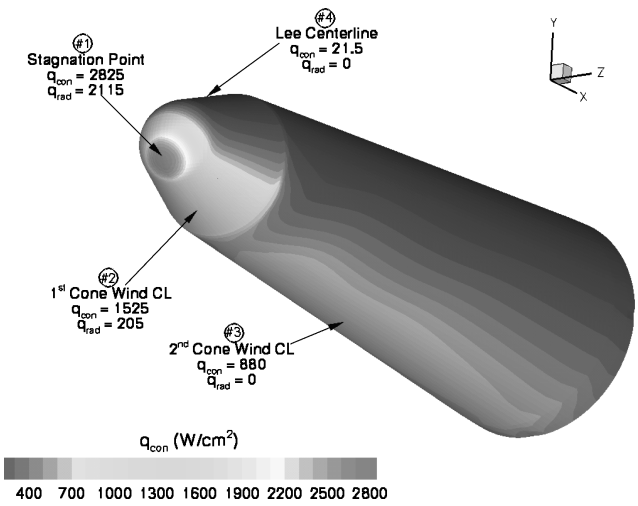

Fig. 10 Computed convective heating rates at the peak heating point ($t = 304$ s) of the overshoot trajectory. Arrows indicate peak convective q_{con} and radiative q_{rad} heating rates at each of the four points selected for TPS sizing analysis.

Additional heating caused by shock-layer radiation transmitted to the surface is computed using NEQAIR,[17] assuming a tangent slab approximation. The primary sources of shock-layer radiation are the atomic lines of the hydrogen atom and the bound–free and free–free (Brehmstraalung) continua.

To make an estimate of the likelihood of turbulent transition, a standard transition criterion ($Re_\theta/M_e < 250$) is applied.[18] Based on this criterion, the flowfield will remain laminar on the wind side of the vehicle throughout the aeropass on all three trajectories. Turbulence is likely on the lee side because of crossflow separation, but the heat loads are so small on the lee side that turbulent heating will not significantly increase TPS mass, and so it is neglected in this preliminary analysis. Turbulent transition could also be initiated on the wind side by roughness or blowing caused by ablation of the TPS material, but this effect was considered beyond the scope of this work.

Figure 10 shows the convective heating rate distribution on the surface of the vehicle for the overshoot trajectory peak heating condition ($t = 304$ s). Surface convective heating varies from 2840 W/cm^2 at the stagnation point to only 4 W/cm^2 on the lee side. Also shown in Fig. 10 is the computed peak convective and radiative heating at each of the four body points for which a TPS sizing is to be performed. Although the radiative heating at the stagnation point is nearly as large as the convective ($q_{\text{rad}} = 2125$ W/cm^2), the radiative heating falls off rapidly away from the stagnation region and is negligible on the second cone and the entire lee side of the vehicle. The heating distribution for the other cases simulated is qualitatively similar.

Tables 2 and 3 show the convective and radiative heat loads on the vehicle at each of the four TPS sizing points for all three trajectories. From the tables we see that both the bank (1B) and AOA (1A) modulated trajectories have a total heat load of slightly more than half of the overshoot trajectory. This result demonstrates the utility of using robust trajectory analysis for TPS design rather than the traditional overshoot approach. The ratio between the stagnation-point convective heat loads on trajectories 1A and 1B to the overshoot value is in excellent agreement with that predicted using the air correlation in POST, which justifies the use of normalized POST heating correlations for the determination of the worst-case heating trajectories. The heat loads for trajectory 1A are in general slightly lower than those for trajectory 1B, with the exception of the radiative heating at point #2, which is five times higher on trajectory 1A. This result is because of a combination of a higher angle of attack on trajectory 1A during the peak heating period (41 vs 34 deg), which leads to a stronger shock wave on the wind side, coupled with the strong dependence of shock-layer radiation on the postshock temperature of the gas. As expected, the impact of radiation is essentially confined to the stagnation region and wind side of the first cone. Also note from the tables that the peak heat load on the lee side of the vehicle is less than 1% of the stagnation-point heating.

Table 2 Convective heat loads at all TPS sizing points for the three simulated trajectories

TPS sizing point	Overshoot	Q_{con}, kJ/cm^2 bank mod. (1B)	AOA mod. (1A)
1	1150	675	580
2	590	350	330
3	330	190	200
4	9.9	5.8	4.5

Table 3 Radiative heat loads at all TPS sizing points for the three simulated trajectories

TPS sizing point	Overshoot	Q_{rad}, kJ/cm^2 bank mod. (1B)	AOA mod. (1A)
1	550	200	190
2	65	21	130
3	0.03	0.005	0.02
4	0	0	0

Table 4 TPS thickness at all TPS sizing points for the three simulated trajectories

TPS sizing point	Overshoot	Thickness, cm bank mod. (1B)	AOA mod. (1A)
1	12.73	8.35	7.75
2	7.60	5.94	6.13
3	6.72	5.05	4.99
4	3.13	2.53	2.15

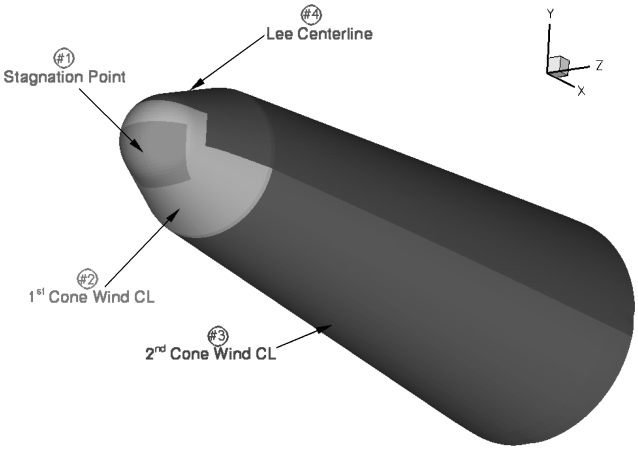

Fig. 11 Approximate TPS splitlines based on the four sizing points.

The computed heat rates were used as input to the material response analysis code FIAT (fully implicit ablation and thermal response)[19] to determine the required TPS thickness. FIAT is a program for the simulation of one-dimensional transient thermal energy transport in a multi-layer stack of isotropic materials and structure that can ablate from a front surface and decompose in depth. The carbon-phenolic material properties used in the FIAT simulation are taken from the work of Laub and Beck.[7] The required mass loss (B-prime) tables were generated using the aerotherm chemical equilibrium code[20] for carbon-phenolic and the Neptune atmosphere composition. The initial TPS temperature is assumed to be -33°C, and the back face of material is assumed to be adiabatic (no conduction into the underlying structure), which provides a reasonable yet conservative TPS sizing. The zero-margin TPS thickness is obtained as the backface maximum temperature reaches 250°C at the point in the trajectory when the vehicle returns to 1000 km after the completion of the aeropass. After returning to a 1000-km altitude, the heat shield is assumed to be jettisoned, which eliminates further heat soak.

Table 4 shows the computed carbon-phenolic TPS thickness at all four TPS sizing points for each of the simulated trajectories. The required TPS thickness at the stagnation point decreases by about 34% from the overshoot value for the bank modulated trajectory (1B) and 39% for the angle-of-attack modulated trajectory (1A). The reduction in TPS thickness at the other sizing points is slightly less, averaging about 21% for trajectories 1A and 1B. The required thickness is slightly lower for trajectory 1A than for 1B at three of the four sizing points. The exception is point #2, where the large increase in radiative heat load on trajectory 1A vs 1B more than offsets the small decrease in convective heating. Finally the TPS on the leeward side is quite thick given the small heat load. This apparent anomaly is because in this region the heating rates are so low that the carbon-phenolic is not ablating, but is acting primarily as an (inefficient) insulator.

As a preliminary estimate of the TPS mass, we assume that the vehicle is divided into four regions as shown in Fig. 11, each with a constant thickness of carbon phenolic TPS material. Assuming a density for fully dense carbon phenolic of 1.45 g/cm^3 (Ref. 7), the TPS mass for each region shown in Fig. 11 is given in Table 5. From the table we see that for the overshoot trajectory, 517 kg of carbon phenolic is required, which equates to a mass fraction of 86% for

Table 5 Surface area and TPS mass of each region of the heat shield for the three simulated trajectories

TPS sizing point	Area, m^2	Overshoot	TPS mass, kg bank mod. (1B)	AOA mod. (1A)
1	0.104	19	13	12
2	0.347	38	30	31
3	2.868	280	210	208
4	3.966	180	145	124
Total	7.284	517	398	374

the TPS material alone. When the additional mass of the supporting structure is included, it is clear that the mass fraction of this aeroshell would exceed unity. The situation is better for the bank and AOA modulated trajectories (398 and 374 kg, respectively). However, these results show that for all entry cases evaluated in this study TPS masses calculated for Neptune aerocapture represent a significant fraction of vehicle's total 600-kg entry mass. Therefore, the 23% reduction in TPS mass achieved for the bank-modulated robust trajectory relative to TPS mass of the overshoot case represents a significant improvement in aerobraking TPS efficiency and can in fact be enabling for certain mission classes. The addition of angle-of-attack modulation allows a moderately larger TPS mass reduction of 28% relative to the overshoot trajectory. Table 5 also demonstrates that stagnation-point heat load is not the best design driver to use for trajectory analysis. The addition of angle-of-attack modulation resulted in an additional 10% decrease in stagnation-point heat load over the bank modulated case, but this only translated into a 1-kg reduction in TPS mass because the stagnation area is small. A potentially better metric would be to monitor the heat load at several points on the vehicle, but this requires engineering correlations of distributed heating for Neptune, which were not available for this study.

From Table 5 it is clear that significant weight savings could be achieved by varying the material selected on various areas of the vehicle, as demonstrated in Ref. 14. TPS based entirely on carbon-phenolic is a simplistic approach from a materials point of view. Figure 10 demonstrates that there are large areas on the vehicle where heating rates are more than an order of magnitude lower than those in the stagnation region. In these areas a lower-density material that is a better insulator would be a better choice than fully dense carbon-phenolic. The selection and sizing of multiple TPS materials was beyond the scope of the present study, but these results do indicate that it is likely that a more detailed analysis of the Neptune aerocapture problem with multiple materials and carefully selected split lines would result in a significant reduction in the TPS mass fraction. For example, the largest area of the aeroshell in Fig. 11 is the lee side (region #4). The TPS mass in this region, assuming carbon-phenolic, is about 35% of the total. Switching to a low-mass alternative for this portion of the aeroshell could result in a factor of two or greater reduction in overall TPS mass of this region.

Summary

The application of nominal-robust trajectory design applied in this study to a Neptune aerocapture mission demonstrates that TPS thickness, and therefore mass fraction, can be significantly reduced compared with traditional undershoot/overshoot TPS design practice. If the nominal trajectory with a properly oriented lift vector is modeled in the presence of realistic dispersions, an aerocapture vehicle with sufficient control authority will never need to fly anywhere near a full overshoot trajectory. For example, for this application the worst-case stagnation-point heat load on any of the off-nominal trajectories, assuming bank modulation only, was about 34% less than that for the overshoot trajectory. The nominal-robust trajectory approach is also much less time consuming than (admittedly more rigorous) Monte Carlo trajectory analysis. Thus, it is recommended that preliminary TPS sizing during the early design phase should be based on the worst case resulting from modeling in the presence of dispersions rather than the full overshoot case. This type of nominal-robust trajectory design would be applicable to any aerocapture or lifting direct entry mission to an atmosphere bearing body.

Further, closed-loop trajectory simulation demonstrates that the addition of AOA modulation allows for additional reduction of integrated heat load than could be achieved through bank-angle modulation only. For the highest heat load trajectories simulated, AOA modulation decreased stagnation-point convective heat load by about 15% and radiative heat load by 5% over a bank-angle-only modulated trajectory. Also, AOA modulation permits more efficient control of the exit apoapse than could be achieved with bank-angle modulation alone. Thus, AOA modulation capability provides a significant guidance enhancement, which in turn allows more efficient constraint of the integrated heat load through the ability to increase vehicle drag and fly at higher altitudes. However, as the high-fidelity TPS sizing analysis shows, optimization of a distributed TPS sizing (as opposed to stagnation point only), particularly for cases with significant shock-layer radiation, is a more complex task that must be carefully considered. It is apparent from the current results that significant weight savings would be possible by tailoring both the TPS material selected and the total thickness to the local aerothermal environment at each point on the vehicle. In fact, the present results suggest that it might not be possible to close the design of a Neptune aerocapture vehicle for some applications without such tailoring.

Perhaps the most important conclusion is that the use of numeric predictor-corrector guidance algorithm demonstrated that robust aerocapture at Neptune can be achieved even for the vehicle capable of bank modulation only. This result is thought to be mainly caused by the flexibility afforded by the guidance scheme, which utilizes four predicted bank angles and three time variable intervals between them as multiple controls to guide the vehicle through the remaining part of the trajectory. Smaller dispersions in postexit ΔV and somewhat smaller TPS materials thickness achieved by addition of AOA modulation into the guidance scheme will have to be carefully weighed against the additional vehicle complexity associated with the implementation of this technology.

References

[1]Lockwood, M. K., "Neptune Aerocapture Systems Analysis," AIAA Paper 2004-4951, Aug. 2004.

[2]Walberg, G. D., "A Review of Aerobraking for Mars Missions," International Astronautical Federation, Paper 88-196, Oct. 1988.

[3]Wercinski, P. F., Chen, Y.-K., Loomis, M., Tauber, M., McDaniel, R., Wright, M., Papadopoulos, P., Allen, G., and Yang, L., "Neptune Aerocapture Entry Preliminary Design," AIAA Paper 2002-4812, Aug. 2002.

[4]Starr, B. R., Westhelle, C. H., and Masciarelli, J. P., "Aerocapture Performance Analysis for a Neptune Triton Exploration Mission," AIAA Paper 2004-4955, Aug. 2004.

[5]Jits, R. Y., "Trajectory Analysis for Thermal Protection System Design of Mars Aerocapture Vehicles," AIAA Paper 2002-0818, Jan. 2002.

[6]Jits, R. Y., Chen, Y.-K., and Wright, M. J., "Trajectory Analysis for Thermal Protection System Design of Neptune Aerocapture Vehicle," International Astronautical Federation, Paper IAC-02-Q.2.06, Oct. 2002.

[7]Laub, B., and Beck, R., "Development of Baseline Response Model for Carbon Phenolic," ITT Aerotherm, Contract GS-23F-010K, Mountain View, CA, Oct. 2000.

[8]Brauer, G. L., Cornick, D. E., Habeger, A. R., Petersen, F. M., and Stevenson, R., "Program to Optimize Simulated Trajectories (POST)," NASA CR-132691, April 1975.

[9]Rousseau, S., Perot, E., Graves, C., Masciarelli, J., and Queen, E., "Aerocapture Guidance Algorithm Comparison Campaign," AIAA Paper 2002-4822, Aug. 2002.

[10]Masciarelli, J. P., Westhelle, C. H., and Graves, C. A., "Aerocapture Guidance Performance for the Neptune Orbiter," AIAA Paper 2004-4954, Aug. 2004.

[11]Hollis, B. R., Wright, M. J., Olejniczak, J., Takashima, N., Sutton, K., and Prabhu, D. K., "Preliminary Convective-Radiative Heating for a Neptune Aerocapture Mission," AIAA Paper 2004-5177, Aug. 2004.

[12]Jits, R. Y., and Walberg, G. D., "Blended Control, Predictor-Corrector Guidance: An Enabling Technology for Mars Aerocapture," *Acta Astronautica*, Vol. 54, No. 6, 2004, pp. 385–398.

[13]Bishop, J., Atreya, S., Romani, P., Sandel, B., and Yelle, R., "The Middle and Upper Atmosphere of Neptune," *Neptune*, edited by D. Cruikshank, Univ. of Arizona Press, Tucson, AZ, 1995, pp. 427–489.

[14]Laub, B., and Chen, Y.-K., "TPS Challenges for Neptune Aerocapture," AIAA Paper 2004-5178, Aug. 2004.

[15]Wright, M. J., Candler, G. V., and Bose, D., "A Data Parallel Line Relaxation Method for the Navier–Stokes Equations," *AIAA Journal*, Vol. 36, No. 9, 1998, pp. 1603–1609.

[16]Leibowitz, L. P., and Kuo, T. J., "Ionizational Nonequilibrium During Outer Planetary Entries," *AIAA Journal*, Vol. 14, No. 9, 1976, pp. 1324–1329.

[17]Whiting, E. E., Park, C., Liu, Y., Arnold, J. O., and Paterson, J. A., "NEQAIR96, Nonequilibrium and Equilibrium Radiative Transport and Spectra Program: Users Manual," NASA RP-1389, Dec. 1996.

[18]Tauber, M. E., "A Review of High-Speed Convective Heat Transfer Computation Methods," NASA TP-2914, July 1989.

[19]Chen, Y.-K., and Milos, F. S., "Ablation and Thermal Response Program for Spacecraft Heatshield Analysis," *Journal of Spacecraft and Rockets*, Vol. 36, No. 3, 1999, pp. 475–483.

[20]"Users Manual: Aerotherm Chemical Equilibrium Computer Program (ACE 81)," Acurex Corp., Acurex Rept. UM-81-11/ATD, Mountain View, CA, Oct. 1974.

P. Huseman
Associate Editor